Ultrasound-assisted synthesis of porous $Mg(OH)_2$ nanostructures using hypersaline brine

Sadegh Yousefi ✉, *Behrooz Ghasemi*

Faculty of Metallurgy and Materials Science, Semnan University, Semnan 35131-19111, Iran
✉ *E-mail: s.yousefi@semnan.ac.ir*

Published in Micro & Nano Letters; Received on 19th January 2019; Revised on 17th March 2019; Accepted on 30th April 2019

In this work, synthesis and formation of porous magnesium hydroxide (MH) nanostructures were investigated by chemical precipitation and sonochemical method using hypersaline brine containing large amounts of $CaCl_2$, $MgCl_2$, NaCl and KCl. The effect of ultrasound waves was investigated on the morpho-structural, surface and thermal properties were investigated by means of X-ray diffraction, field emission scanning electron microscopy, transmission electron microscopy, energy dispersive X-ray spectrometer, Brunauer–Emmett–Teller and thermogravimetry-differential thermal analysis techniques. It was indicated that ultrasound waves decreased grain and particle sizes of the sample which synthesised by sonochemical route (MH-U). The MH-U sample had a higher surface area, lower particle size, better particle distribution and lower transition temperature of MH to MgO.

1. Introduction: Magnesium hydroxide (MH) nanoparticles have been attracting much attention owing to extensive use in many fields like in catalysts support, sorbent for chemical and destructive adsorption of diverse pollutants, plastic rubber, wood pulp bleaching, neutralisation of acid wastewater, fertilizer additive, pharmacy, biomaterials, fire-retardant materials because of their unique physical and chemical properties [1–4]. In recent years, MH nanostructures with various morphologies have been successfully synthesised by different approaches and by use of different preparation conditions such as chemical precipitation method [1], sol–gel [5], hydrothermal [6, 7], solvothermal [8], microwave [9] and ultrasound-assisted synthesis [10–12]. Sonochemical synthesis organises a new and economical way for the synthesis of nanostructures without extra reagents and time-consuming chemistry and compared with other methods, the sonochemical route does not require the use of high temperatures, and enables elimination of the problem of control of process parameters, such as pH and pressure [2]. In this method, the main phenomenon is the acoustic cavitation, which leads to the formation, growth, and collapse of bubbles in the liquid [13]. Cavitation-induced sonochemistry provides a unique interaction between energy and matter, with hot spots inside the bubbles of 5000 K, pressures of 1000 bar, heating and cooling rates of $>10^{10}$ K s^{-1}; these special conditions permit access to a range of chemical reaction space normally not accessible, which allows for the synthesis of a wide range of nanostructured materials [14].

In previous studies of sonochemical synthesis of MH nanostructures, Alavi and Morsali synthesised MH nanostructures with a low surface area by the reaction of magnesium acetate with NaOH via the sonochemical method and results indicated that the ultrasonic irradiation increases the surface area of the MH particles [10]. Song *et al.* prepared successfully hydrophobic MH nanoparticles using $MgCl_2{\cdot}6H_2O$ and an organic phase via one-step precipitation reaction with the assist of ultrasonic treatment [11]. They illustrated that Tween 80 was favourable to obtain smaller sized MH nanoparticles with even crystal growth and better dispersibility, and to further enhance the hydrophobic property of MH nanoparticles based on its bridging function between the surface of MH nanoparticles and aliphatic compounds in the organic phase. Baidukova and Skorb obtained nanosize MH platelet-shaped, from pure magnesium and without the requirement of any additives and non-aqueous solvents [12]. In all of the above-mentioned works and similar attempts, the use of pure raw material containing magnesium (such as $MgCl_2$, $Mg(NO_3)_2$, $MgSO_4$ etc.) is essential to synthesise MH nanoparticles. In our previous study, MH nanoplates have been successfully synthesised from impure brine without any surfactant by a chemical precipitation method for the first time [15]. We demonstrated that MH nanostructures had high purity and good optical properties although they were synthesised from impure magnesium precursor (brine).

In this work, we reported a facile method for the synthesis of porous and high specific surface area (SSA) MH nanostructures using same impure brine with the sonochemical method in the presence of polyethylene glycol (PEG) 4000. To the best of our knowledge, ultrasonic-assisted synthesis of MH nanoparticles in one-step precipitation using hypersaline brine not reported and no previous studies have explored the synthesis of porous MH nanostructures using impure brine and sonochemical method. The synthesised MH nanoparticles were characterised by X-ray diffraction (XRD), field emission scanning electron microscopy (FESEM), transmission electron microscopy (TEM), energy dispersive X-ray spectrometer (EDS), Brunauer–Emmett–Teller (BET), and thermogravimetry-differential thermal analysis (TG-DTA).

2. Experimental

2.1. Chemicals and materials: Polyethylene glycol (PEG 4000), NaOH and ethanol were purchased from Merck and used without further purification. De-ionised water was utilised throughout this work. The chemical composition of used brine in this study was the same hypersaline brine in our previous work [11].

2.2. Preparation of MH nanostructures: In a typical synthesis (according to Fig. 1), 8.72 g of NaOH and PEG 4000 were dissolved in 73 ml de-ionised water for 10 min under vigorous stirring to form a transparent solution. Then, the prepared solution was added drop by drop into a beaker containing 50 cc brine under ultrasonic irradiation at 100 W (20 kHz). Chemical stability of $Mg(OH)_2$ complexes ($MgOH^+$ and $[Mg_4(OH)_4]^{4+}$) and control of reaction pH were investigated using equilibrium diagrams with MEDUSA software (http://www.kemi.kth.se/medusa) and the hydrochemical equilibrium-constant database (HYDRA) in order to establish the experimental conditions. To prevent the formation of calcium hydroxide ($Ca(OH)_2$) during synthesis, pH was kept at 9–9.5 range (Fig. 2). Then, the resulting white precipitates were collected by vacuum filtration and washed by absolute ethanol and de-ionised water for several times.

© The Institution of Engineering and Technology 2019

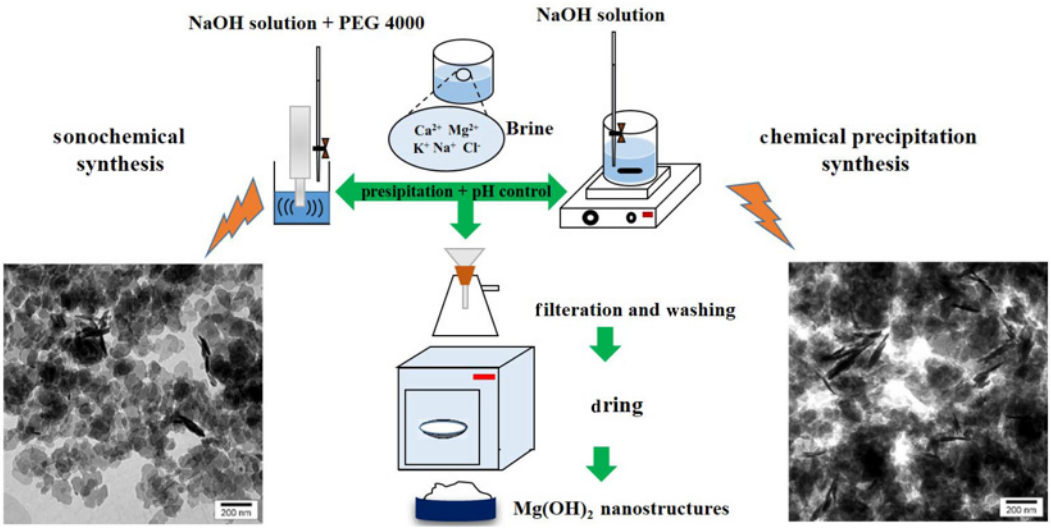

Fig. 1 *Schematic diagram for synthesis of $Mg(OH)_2$ nanoparticles using chemical precipitation and sonochemical routes*

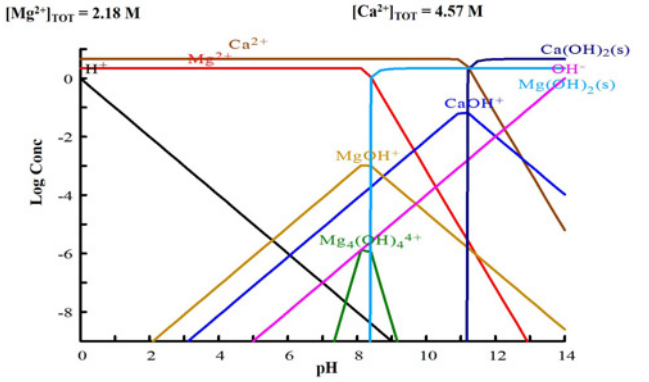

Fig. 2 *pH versus log concentration plot for a fixed $[Mg^{2+}] = 2.18$ M and $[Ca^{2+}] = 4.57$ M to avoid formation of $Ca(OH)_2$ during $Mg(OH)_2$ synthesis*

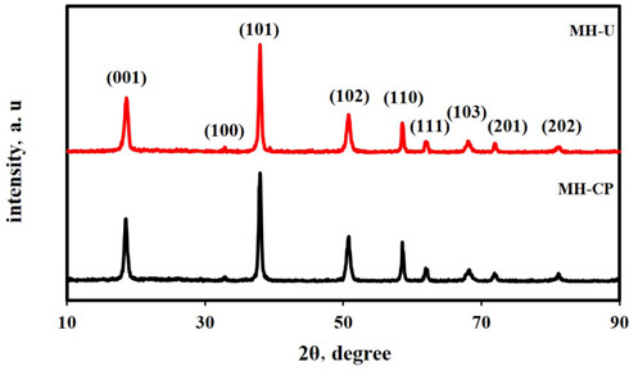

Fig. 3 *XRD patterns of as-synthesised $Mg(OH)_2$ nanostructures*

The final cake was dried in an oven at 125°C for 1 h (sample MH-U).

To study the effect of ultrasonic irradiation an experiment was carried out by chemical precipitation route in the absence of waves and PEG 4000 under vigorous stirring (sample MH-CP). The samples were collected for subsequent characterisations.

2.3. Characterisations: The powder XRD patterns were characterised on a Bruker X-ray diffractometer (D8 Bruker, CuKα, $\lambda = 1.5406$ Å, Germany). The morphologies of products were examined by (FESEM, MIRA3, TE-SCAN) equipped with an EDS and transmission electron microscopy (TEM, LEO912-AB). FTIR spectra were recorded on a TENSOR 27 (Brucker, Germany) infrared. The BET surface area analysis was measured on Micromeritics ASAP 2020 (American) instrument. Also, thermal analysis was carried out using VT30-LINSIES instrument at a heating rate of 10°C min^{-1}.

3. Results and discussion: Fig. 3 indicates the XRD patterns of the MH samples synthesised under different synthesis route. All the marked peaks can be assigned to a pure phase of brucite $Mg(OH)_2$ (JCPDS Card No. 7-0239). The average crystallite size of prepared MH samples was calculated by Scherrer's formula [16]. The XRD study demonstrated that the grain size of MH-U and MH-CP were 22 and 19 nm, respectively.

The characteristic N_2 adsorption–desorption isotherms for the synthesised MH samples are illustrated in Fig. 4*a*. The nitrogen adsorption–desorption profiles for both samples could be classified as type-IV with H3 hysteresis loop according to the IUPAC standard, which is corresponded with slit-like pores. This type of hysteresis is associate to solids including of accumulates or agglomerates of particles making slit-shaped pores (plates or edged particles like cubes), containing a non-uniform size and/or shape [17]. Also, the theoretical particle sizes were estimated from surface area, assuming spherical particles, using the following equation [18]:

$$D_{BET} = 6000/(\rho \times S) \quad (1)$$

where D_{BET}, ρ and S are the equivalent particle diameter (nm), the density of the sample (g cm^{-3}) and the specific surface area (m^2 g^{-1}), respectively. These results are shown in Table 1.

As seen, ultrasound irradiation decreases the crystallite size (CS) and increases the SSA of MH sample. As is clear, the D_{BET} decreases by using ultrasonic waves. Due to broken of particles in the early stages of synthesis, using ultrasonic radiation decreased the agglomeration and average particle size. Therefore, by reducing the particle size, increased the SSA of MH-U sample.

The average pores size distribution of synthesised MH samples that was determined by the Barrett–Joyner–Halenda method (using the desorption branch) are shown in Fig. 4*b*. The pore structure parameters of the MH products are listed in Table 1. The data

© The Institution of Engineering and Technology 2019

doi: 10.1049/mnl.2019.0047

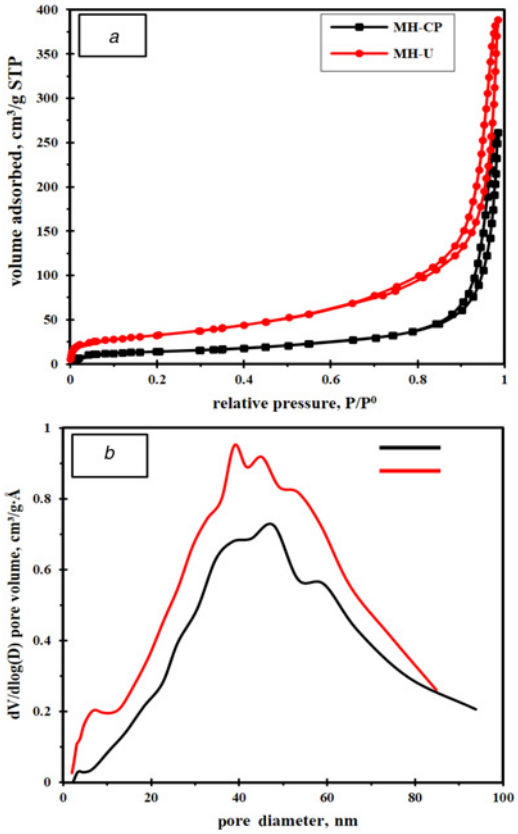

Fig. 4 *Results of BET test*
a N_2 adsorption–desorption of MH-CP and MH-U nanoparticles
b Pore diameter distribution of as-synthesised nanoparticles

Table 1 Structural properties of synthesised MH samples

Sample	MH-CP	MH-U
average crystallite size, nm	22	19
S_{BET}, m^2/g	47.74	116.30
pore volume, cm^3/g	0.39	0.57
average pore size, nm	26.30	16.59
D_{BET}, nm	53.03	21.76

available in this table indicate that the SSA and pores volume of the MH-U sample significantly is increased by using sonochemical synthesis, while the average distribution of pore size has decreased. In addition, the mesoporous structure of MH samples is proved by the information in Table 1 and Fig. 4.

The morphologies of synthesised MH were examined by TEM and FESEM analysis. The FESEM and TEM images of the as-synthesised MH samples are shown in Fig. 5. The presence of MH nanoplates that are agglomerated due to high surface energy is evident in these images. As it is clear, the particles agglomeration in MH-U sample is relatively lower than MH-CP sample and the wide nanoplates are parsed into flakes due to the effect of ultrasonic waves. In addition, the presence of pores with different sizes in parts of the microstructure of the samples, especially between the plates, is evident. The microscopic observations are in good agreement with BET test. Reduction of agglomeration in MH-U sample can be attributed to the presence of PEG. The growth mechanism of magnesium hydroxide nanoplates from brine (Yousefi's model [15]) is shown in Fig. 6. Adsorption of PEG surfactant on the $Mg(OH)_2$ nuclei minimises the surface energy of MH layers, resulting in the flat lamellar-like MH crystals. More information about the

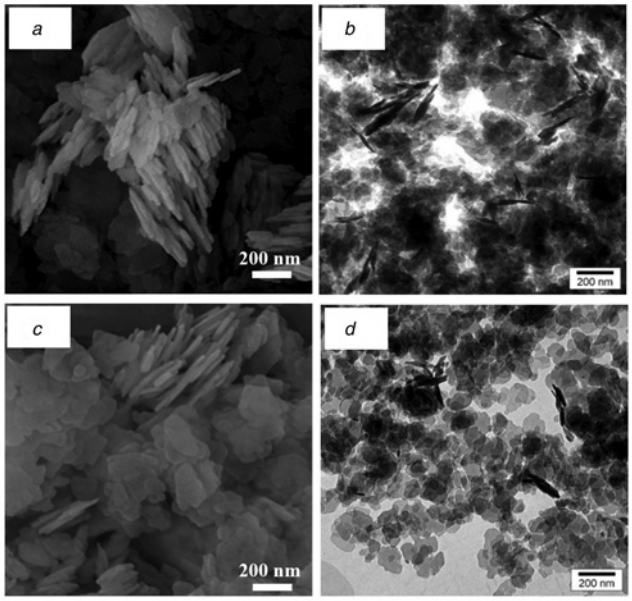

Fig. 5 *FESEM and TEM images for $Mg(OH)_2$ nanoplates*
a FESEM image of MH-CP sample
b TEM image of MH-CP sample
c FESEM image of MH-U sample
d TEM image of MH-U sample

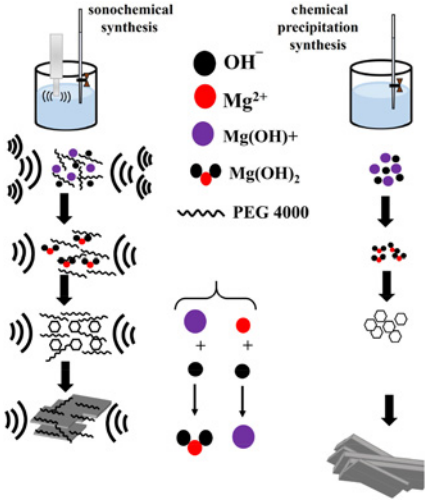

Fig. 6 *Formation mechanism of $Mg(OH)_2$ nanostructures by chemical precipitation and sonochemical routes*

role of PEG on the morphology and growth of MH nanostructured is mentioned in the literature [1, 4, 16]. Also, Cl^- ions in solution brine can act as capping reagent and presence of Cl^- not only increases the reaction rate between Mg^{2+} and OH^- ions but also leads to the formation of 2D $Mg(OH)_2$ nanostructures (nanoplates) [19]. Moreover, the morphologies of this $Mg(OH)_2$ nanostructures formed are dependent on Cl^- concentration which due to the high concentration of Cl^- ions in the brine, the morphology is nanoplate. These ions play a similar role with PEG, where the adsorption of Cl^- should occur on the site of $Mg(OH)^+$ because of the negative charge of Cl^- and absorbs on high-density planes which causes the plate-like growth of nanoparticles.

Fig. 7 indicates typical EDS spectra of MH-CP and MH-U nanostructures. As can be seen, only Mg and O peaks present in the prepared products that indicate the obtained MH nanostructures

© The Institution of Engineering and Technology 2019

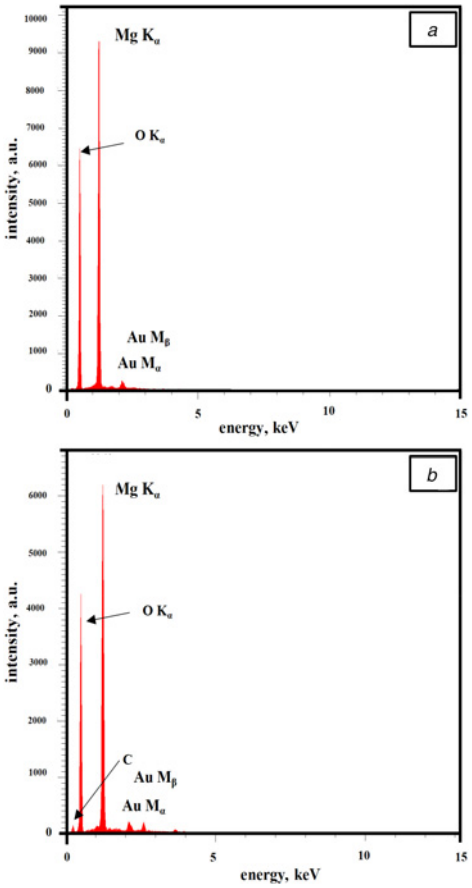

Fig. 7 *EDS spectra of as-synthesised MH samples*
a MH-CP sample
b MH-U sample

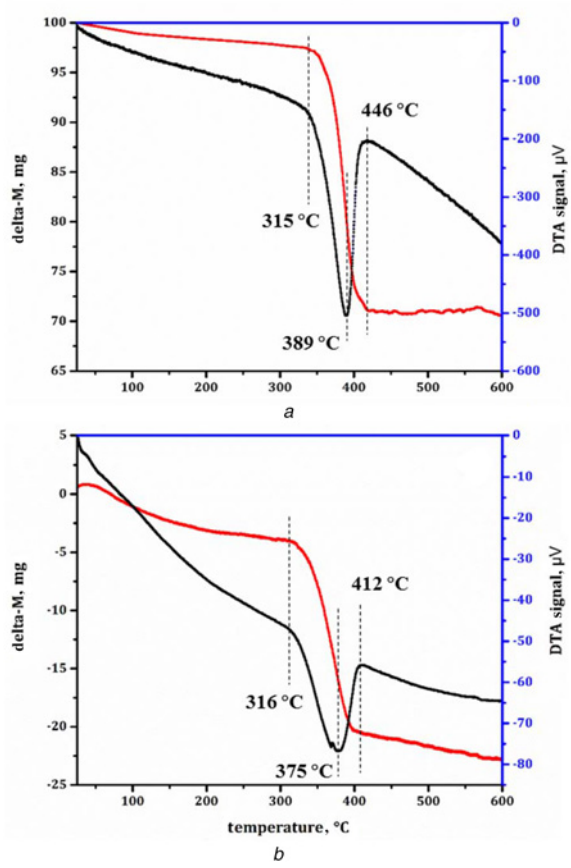

Fig. 8 *DTA-TGA profiles of $Mg(OH)_2$ nanoplates*
a MH-CP sample
b MH-U sample

are without any impurity. The C peak in MH-U sample is associated to the presence of PEG 4000. Therefore, both XRD and EDS analyses represented high purity of MH nanostructures.

TG/DTA profiles of MH-CP and MH-U are shown in Fig. 8. Initial weight loss (2.8%) in MH-CP sample (Fig. 8*a*) is due to water removal, while this weight loss (4.8%) is corresponded to the withdrawal of water and PEG4000 for MH-U sample (Fig. 8*b*) during the first heating stages. The heavy weight loss observed in the TGA profiles shown in the DTA charts as an endothermic peak is due to the MH decomposition and its conversion to MgO (reaction 2) [20]

$$Mg(OH)_2 \xrightarrow{\Delta} \mathrm{MgO} + \mathrm{H_2}O \tag{2}$$

As shown (Fig. 8*a*), the MH-CP sample indicates a pronounced weight loss step within the temperature range of 315–446°C with a total percentage of weight loss of 22.16%, which can be attributed to the decomposition of MH, accompanied by an endothermic peak at 489°C. The thermal behaviour and weight loss at the decomposition stage is different for MH-U sample and the decomposition temperature range of MH to MgO reaches 316–412°C that the total weight loss and the decomposition temperature are down to 16.58% and 375°C, respectively. These results are in agreement with the achievements in previous works [15, 21–23].

Comparison of the thermal behaviour of the MH-U and MH-CP samples show that the use of ultrasonic waves has reduced the temperature range and the conversion temperature of MH to MgO, which is due to the effect of sonochemical synthesis on reducing the particle size. It should be emphasised that the amount of MH weight loss is slightly lower than the theoretical weight loss of 30.8% due to the nanostructure nature of MH particles [3].

4. Conclusion: In this study, $Mg(OH)_2$ nanoflakes were successfully synthesised via chemical precipitation and sonochemical methods. The effect of ultrasound irradiation was investigated on the morphological, structural, surface and thermal properties of $Mg(OH)_2$ nanostructures synthesised from impure brine. XRD and microscopic studies (FESEM and TEM) proved that the synthesised nanoparticles were well produced and sonochemical synthesis reduced grain size, particle size and particle agglomeration. In addition, BET results showed that the SSA and pores volume increased in the sonochemical-synthesised sample (MH-U). This research proved that the sonochemical method is more suitable synthesis route compared to chemical precipitation, with high surface area (116.30 m^2/g), smaller particle size (21.76 nm) and better particle size distribution.

5. Acknowledgment: The authors are grateful to M. Ali Pour for her great help.

6 References

[1] Zheng J., Zhou W.: 'Solution-phase synthesis of magnesium hydroxide nanotubes', *Mater. Lett.*, 2014, **127**, pp. 17–19
[2] Pilarska A.A., Klapiszewski Ł., Teofil J.: 'Recent development in the synthesis, modification and application of $Mg(OH)_2$ and MgO: a review', *Powder Technol.*, 2017, **319**, pp. 373–407
[3] Wang X., Pang H., Chen W., *ET AL.*: 'Controllable fabrication of high purity $Mg(OH)_2$ nanoneedles via direct transformation of natural brucite', *Mater. Lett.*, 2014, **120**, pp. 69–72

© The Institution of Engineering and Technology 2019

doi: 10.1049/mnl.2019.0047

[4] Wang Q., Li C., Guo M., *ET AL.*: 'Hydrothermal synthesis of hexagonal magnesium hydroxide nanoflakes', *Mater. Res. Bull.*, 2014, **51**, pp. 35–39
[5] Minami H., Kinoshita K., Tsuji T., *ET AL.*: 'Preparation of highly crystalline magnesium oxide and polystyrene/ magnesium hydroxide composite particles by sol–gel processes in an ionic liquid', *J. Phys. Chem. C.*, 2014, **116**, (27), pp. 14568–14574
[6] Sabet M., Salavati-niasari M., Asgari Fard Z.: 'Synthesis and characterization of $Mg(OH)_2$ and MgO nanostructures via simple hydrothermal method', *Synth. React. Inorg. Met. Nano-Met. Chem.*, 2016, **46**, (5), pp. 681–686
[7] Treviño P., Perez-robles J.F., Millan-malo B., *ET AL.*: 'Synthesis conditions of $Mg(OH)_2$ nanostructures by hydrothermal route', *Micro Nano Lett.*, 2017, **12**, (6), pp. 404–407
[8] Chen H., Xu C., Liu Y., *ET AL.*: 'Formation of flower-like magnesium hydroxide microstructure via a solvothermal process', *Electron. Mater. Lett.*, 2012, **8**, (5), pp. 529–533
[9] Beall G.W., Duraia E.S.M., El-Tantawy F., *ET AL.*: 'Rapid fabrication of nanostructured magnesium hydroxide and hydromagnesite via microwave-assisted technique', *Powder Technol.*, 2013, **234**, pp. 26–31
[10] Alavi M.A., Morsali A.: 'Syntheses and characterization of $Mg(OH)_2$ and MgO nanostructures by ultrasonic method', *Ultrason. Sonochem.*, 2010, **17**, (2), pp. 441–446
[11] Song G., Ma S., Tang G., *ET AL.*: 'Ultrasonic-assisted synthesis of hydrophobic magnesium hydroxide nanoparticles', *Colloids Surf. A, Physicochem. Eng. Aspects*, 2010, **364**, (1–3), pp. 99–104
[12] Baidukova O., Skorb E.V.: 'Ultrasound-assisted synthesis of magnesium hydroxide nanoparticles from magnesium', *Ultrason. Sonochem.*, 2016, **31**, pp. 423–428
[13] Arruda L.B., Orlandi M.O., Lisboa-Filho P.N.: 'Morphological modifications and surface amorphization in ZnO sonochemically treated nanoparticles', *Ultrason. Sonochem.*, 2013, **20**, (3), pp. 799–804
[14] Bang J.H., Suslick K.S.: 'Applications of ultrasound to the synthesis of nanostructured materials', *Adv. Mater.*, 2010, **22**, (10), pp. 1039–1059
[15] Yousefi S., Ghasemi B., Tajally M., *ET AL.*: 'Optical properties of MgO and $Mg(OH)_2$ nanostructures synthesized by a chemical precipitation method using impure brine', *J. Alloys Compd.*, 2017, **711**, pp. 521–529
[16] Ma X., Ma H., Jiang X., *ET AL.*: 'Preparation of magnesium hydroxide nanoflowers from boron mud via anti-drop precipitation method', *Mater. Res. Bull.*, 2014, **56**, pp. 113–118
[17] Meshkani F., Rezaei M.: 'Effect of process parameters on the synthesis of nanocrystalline magnesium oxide with high surface area and plate-like shape by surfactant assisted precipitation method', *Powder Technol.*, 2010, **199**, (2), pp. 144–148
[18] Rezaei M., Khajenoori M., Nematollahi B.: 'Synthesis of high surface area nanocrystalline MgO by pluronic P123 triblock copolymer surfactant', *Powder Technol.*, 2011, **205**, (1–3), pp. 112–116
[19] Liu Z., Chen J., Zheng Y.: 'Room-temperature synthesis of $Mg(OH)_2$ nanorods and nanowires in Mg–H_2O–NaCl reaction system', *Micro Nano Lett.*, 2013, **8**, (2), pp. 74–77
[20] Mbarki R., Madhi I., M'nif A., *ET AL.*: 'Polyethylene glycol ratio effect on magnesium oxide prepared by chemical precipitation: impact on structure, morphology, and electrical properties', *Mater. Sci. Semicond. Process.*, 2015, **39**, pp. 119–131
[21] Dhaouadi H., Touati F.: '$Mg(OH)_2$ nanorods synthesized by a facile hydrothermal method in the presence of CTAB', *Nano-Micro Lett.*, 2011, **3**, (3), pp. 153–159
[22] Chanda D.K., Das P.S., Samanta A., *ET AL.*: 'Intertwined nanopetal assembly of $Mg(OH)_2$ powders', *Ceram. Int.*, 2014, **40**, (7), pp. 11411–11417
[23] Sierra-Fernandez A., Gomez-Villalba L.S., Milosevic O., *ET AL.*: 'Synthesis and morpho-structural characterization of nanostructured magnesium hydroxide obtained by a hydrothermal method', *Ceram. Int.*, 2014, **40**, (8), pp. 12285–12292

© The Institution of Engineering and Technology 2019